© 2015. Published by The Company of Biologists Ltd | Development (2015) 142, 2478-2486 doi:10.1242/dev.122119

RESEARCH ARTICLE

The *Drosophila* planar polarity gene *multiple wing hairs* directly regulates the actin cytoskeleton

Qiuheng Lu, Dorothy A. Schafer and Paul N. Adler*

ABSTRACT

The evolutionarily conserved *frizzled*/*starry night* (*fz*/*stan*) pathway regulates planar cell polarity (PCP) in vertebrates and invertebrates. This pathway has been extensively studied in the *Drosophila* wing, where it is manifested by an array of distally pointing cuticular hairs. Using *in vivo* imaging we found that, early in hair growth, cells have multiple actin bundles and hairs that subsequently fuse into a single growing hair. The downstream PCP gene *multiple wing hairs* (*mwh*) plays a key role in this process and acts to antagonize the actin cytoskeleton. In *mwh* mutants hair initiation is not limited to a small region at the distal edge of pupal wing cells as in wild type, resulting in multiple hairs with aberrant polarity. Extra actin bundles/hairs are formed and do not completely fuse, in contrast to wild type. As development proceeded additional hairs continued to form, further increasing hair number. We identified a fragment of Mwh with *in vivo* rescue activity and that bound and bundled F-actin filaments and inhibited actin polymerization in *in vitro* actin assays. The loss of these activities can explain the *mwh* mutant phenotype. Our data suggest a model whereby, prior to hair initiation, proximally localized Mwh inhibits actin polymerization resulting in polarized activation of the cytoskeleton and hair formation on the distal side of wing cells. During hair growth Mwh is found in growing hairs, where we suggest it functions to promote the fusion of actin bundles and inhibit the formation of additional actin bundles that could lead to extra hairs.

KEY WORDS: Planar cell polarity, *Drosophila* wing, Actin, Multiple wing hairs

INTRODUCTION

Planar cell polarity (PCP, or tissue polarity) refers to polarity that is oriented along the plane of a group of cells, and in epithelia it is perpendicular to the apical-basal axis of the cells (Adler, 2002; Goodrich and Strutt, 2011; Gubb and Garcia-Bellido, 1982; Tucker, 1981; Vinson and Adler, 1987). Genetic studies identified the *frizzled* (*fz*)/*starry night* (*stan*) pathway as an essential regulator of PCP in a number of *Drosophila* tissues/body regions, such as the wing, eye and abdomen (Adler, 1992; Gho and Schweisguth, 1998; Gubb and Garcia-Bellido, 1982; Held et al., 1986; Lawrence et al., 2004; Vinson and Adler, 1987; Wong and Adler, 1993; Zheng et al., 1995). This pathway also plays a key role in PCP in a variety of vertebrate tissues (and processes), such as the inner ear (Ezan and Montcouquiol, 2013; Montcouquiol et al., 2003; Wang et al., 2005), murine fur (Chang and Nathans, 2013; Wang et al., 2006; Wang and Nathans, 2007), murine respiratory system (Vladar et al., 2012) and mediolateral cell polarization and convergent extension during vertebrate embryogenesis (Goto and Keller, 2002; Heisenberg et al., 2000; Jessen et al., 2002; Tada and Smith, 2000; Wallingford et al., 2001). A second key regulator of PCP is the *dachsous*/*fat* pathway (Adler et al., 1998; Casal et al., 2006; Harumoto et al., 2010; Ma et al., 2003; Matis and Axelrod, 2013; Merkel et al., 2014; Olofsson et al., 2014; Yang et al., 2002), which interacts with the *fz*/*stan* pathway. Additional genes have also been found to be important for fly PCP but how they relate to the *fz*/*stan* genes remains unclear (e.g. Chin and Mlodzik, 2013; Hermle et al., 2013).

The hairs (also known as trichomes) that decorate much of the *Drosophila* epidermis are formed by cytoskeletal-mediated outgrowths. Their planar polarity has been primarily studied in the wing, where the *fz*/*stan* pathway restricts activation of the cytoskeleton to the distal vertex of each cell (Wong and Adler, 1993), resulting in the formation of a single distally pointing hair. Mutations in *fz*/*stan* pathway genes affect the site of hair initiation, adult hair polarity and hair number. The pathway is a hierarchy, with the PCP genes (also known as core genes) acting upstream of the planar cell polarity effector (PPE) genes, which are in turn upstream of *multiple wing hairs* (*mwh*) (Wong and Adler, 1993). *mwh* mutations result in most wing cells forming three or more hairs with aberrant polarity and at abnormal locations along the cell periphery (Strutt and Warrington, 2008; Wong and Adler, 1993; Yan et al., 2008). The multiple hair cell (MHC) phenotype of *mwh* appears to be more sensitive than the polarity phenotype, as at semi-permissive conditions a temperature-sensitive allele of *mwh* results in many cells that form multiple hairs of relatively normal polarity (Yan et al., 2008). All of the proteins produced by the pathway genes accumulate asymmetrically in wild-type pupal wing cells (Adler et al., 2004; Axelrod, 2001; Bastock et al., 2003; Das et al., 2004; Feiguin et al., 2001; Strutt, 2001; Strutt and Warrington, 2008; Usui et al., 1999; Yan et al., 2008).

Growing wing hairs contain both actin filaments and microtubules (Turner and Adler, 1998; Lee and Adler, 2002) that are functionally important. Disruption of either by drug treatment leads to cells forming multiple hairs (Guild et al., 2005; Shimada et al., 2006; Turner and Adler, 1998). In addition, loss-of-function mutations in *Drosophila* actin cytoskeleton regulators, such as the small GTPases *Rho1* and *Cdc42*, the Rho effector *Rho kinase* (*Rok*) and the myosins *crinkled* (myosin VIIa) and *zipper* (myosin II), result in multiple wing hair and hair morphology phenotypes (Eaton et al., 1996; Franke et al., 2010; Kiehart et al., 2004; Winter et al., 2001; Yan et al., 2009). We further studied the role of the actin cytoskeleton in hair outgrowth using *in vivo* imaging and observed that, initially, multiple bundles of F-actin were visible near the distal vertex. Over a period of a couple of hours the bundles merged to form a single hair. The multiple bundles seen early in hair morphogenesis might correspond to the 'pimples' seen in transmission electron microscopy (TEM) studies of wing hair development (Guild et al., 2005).

The structure of the Mwh protein made it a candidate link between the *fz*/*stan* pathway and the actin cytoskeleton as its

Departments of Biology and Cell Biology, University of Virginia, Charlottesville, VA 22904, USA.

*Author for correspondence (pna@virginia.edu)

Received 13 January 2015; Accepted 29 May 2015

Development (2015) 142, 2478-2486 doi:10.1242/dev.122119

N-terminal half showed similarity to Diaphanous (Dia)-related formins (DRFs) (supplementary material Fig. S1), which are a group of actin regulators that promote actin assembly into long filaments (Breitsprecher and Goode, 2013; Campellone and Welch, 2010). Actin assembly by DRFs is mediated by two domains (FH1 and FH2) found in the C-terminal half of Dia that are not found in Mwh. The N-terminal half of DRFs contains a GTPase-binding domain (GBD) and a formin homology 3 domain (FH3) (Kitayama and Uyeda, 2003; Petersen et al., 1994). The GBD-FH3 domain was recently divided into three structural domains: a GBD domain (which is smaller than the region previously identified as the GBD), a diaphanous inhibitory domain (DID), and a dimerization domain (DD) (Goode and Eck, 2007; Harris et al., 2004, 2006; Li and Higgs, 2005; Moseley et al., 2004). Dia activity is inhibited by the intramolecular binding of the C-terminal diaphanous autoregulatory domain (DAD) to the DID (Alberts, 2001; Li and Higgs, 2005). This autoinhibition is relieved by the binding of Rho-GTP to the GBD. It seems likely that the GBD-FH3 domain of Mwh mediates an interaction with Rho-GTP analogous to the interaction between Rho1 and Dia (Yan et al., 2009). Mwh and Rho1 co-immunoprecipitate and Rho1 activity is required for the accumulation of Mwh in wing cells. Positive genetic interactions also exist between the genes. Based on analogy with the interaction of Rho1 with DRFs, it is likely that Rho1 activates Mwh by releasing a potential autoinhibition. BLAST searches of the *Drosophila* genome with a mammalian formin will pick up *mwh* due to the GBD-FH3 domain; however, *mwh* is never the most similar to the mammalian query sequence, so it is not a homolog of any formin.

In contrast to DRFs, several lines of evidence suggest that Mwh acts as an antagonist of the actin cytoskeleton. Mwh localizes to the proximal side of the cell prior to hair initiation (Strutt and Warrington, 2008; Yan et al., 2008), opposite to where the actin cytoskeleton is activated for hair outgrowth. Overexpression of Mwh is able to delay hair initiation in pupal wing cells (Yan et al., 2008) and suppresses the formation of actin filaments in *Drosophila* S2 cells (Strutt and Warrington, 2008). Ectopic actin filaments/bundles are also seen across the apical surface of fixed and stained *mwh* mutant wing cells (Strutt and Warrington, 2008).

Consistent with antagonistic effects on actin, in the present study we observed filamentous actin (F-actin) accumulation at the start of hair formation over a larger part of the apical surface in *mwh* mutant than wild-type cells. We also observed that more actin bundles were formed and the fusion of these bundles was not complete in *mwh* mutant wings. Finally, in *mwh* mutant cells we observed that hair initiation continued for several hours beyond the normal period. All of these factors contributed to the adult MHC phenotype.

How could Mwh function to antagonize the actin cytoskeleton? In principle, it could act directly on F-actin or globular actin (G-actin). Alternatively, it could function by interacting with a regulator of the actin cytoskeleton, such as Dia or the Arp2/3 complex. We tested the former model and found that a fragment of Mwh that had rescue activity *in vivo* inhibited actin polymerization *in vitro*. We further found that Mwh was able to bind to and bundle actin filaments. These activities provide an explanation for the phenotypes of *mwh* mutants.

RESULTS

Hair development in wild-type *Drosophila*

Published images of developing wing hairs usually show fixed, phalloidin-stained (phalloidin specifically stains F-actin) wings at a middle stage of hair growth (Fig. 1E,F). At this stage the hair is well

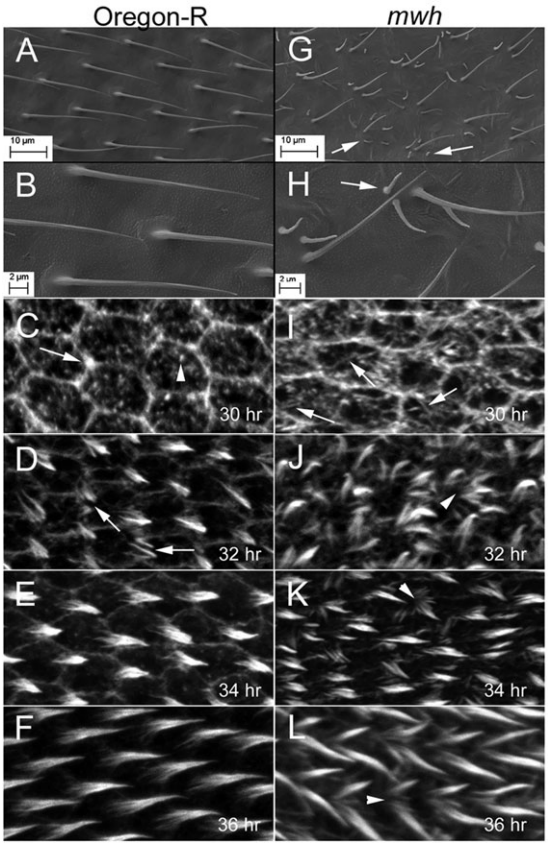

Fig. 1. Comparison of wild-type and *mwh* mutant wings. (A,B) SEM of wild-type (Oregon-R) adult *Drosophila* wings. (C-F) Phalloidin-stained wild-type pupal wings from 30 (C), 32 (D), 34 (E) and 36 (F) h after white prepupae (awp). (C) The arrow points to an area of F-actin accumulation at the cell membrane and the arrowhead an F-actin focus not juxtaposed to the membrane. (D) Arrows point to cells with multiple growing hairs/actin bundles. (G,H) SEM of *mwh*^{1} mutant wings. The arrows point to the very small extra hairs formed in *mwh* mutants. (I-L) Phalloidin-stained *mwh* pupal wings from 30 (I), 32 (J), 34 (K) and 36 (L) h awp. (I) Arrows point to ectopic actin filaments seen in the mutant. (J-L) Arrowheads point to cells with multiple hairs/actin bundles.

formed but not so long as to overlap with hairs formed by more distal cells. Prior to obvious hair initiation we often see regions juxtaposed to the distal membrane that stain brightly for F-actin (Fig. 1C, arrow) and brightly staining foci appear in the apical cortex (Fig. 1C, arrowhead). When a growing hair first becomes obvious it appears as if the length of the growing hair is similar to the length of the 'rootlet' that extends basally and proximally into the cell (supplementary material Fig. S2, arrows). Early in hair extension it often appears that there are 'multiple bundles' of F-actin (Fig. 1D, arrows). At later stages only a single large region (bundle) of F-actin is seen and this appears to fill the hair (Fig. 1E,F). After hair extension is complete the hair moves to the center of the apical surface and is found on a pedestal. A remnant of this pedestal can be seen in scanning electron microscopy (SEM) images of the adult wing (Fig. 1A,B).

How the multiple bundles are refined into the single large one could not be addressed by examining fixed material. To answer this question we imaged the actin cytoskeleton in developing wings. In our initial experiments we drove the expression of *actin-GFP* using *apterous Gal4* (*ap>actin-GFP*). Similar results were obtained from observing *ap>lifeact-GFP* and *sqh-cherry-moesin* pupal wings. Prior to hair initiation we see regions of bright actin staining along the apical/lateral membrane (Fig. 2A-F, arrows and

Development (2015) 142, 2478-2486 doi:10.1242/dev.122119

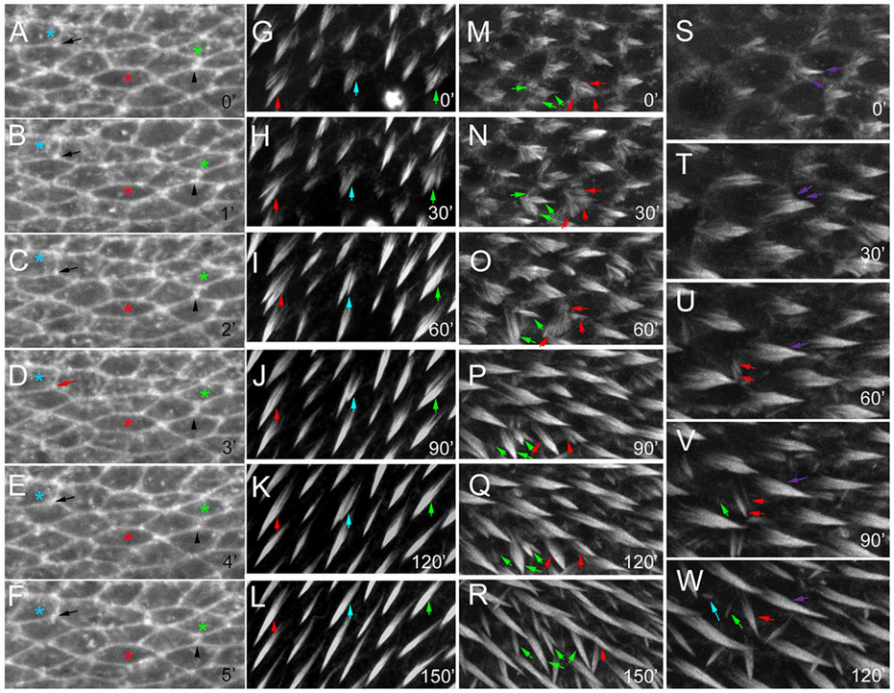

Fig. 2. Time-lapse *in vivo* imaging of actin in pupal wings. In all cases images are maximal projections of 2-3 optical sections. (A-F) *ap>actin-GFP* pupal wing prior to hair initiation (~28 h awp). Images were taken 1 min apart. The blue, green and red asterisks mark cells that contain a brightly staining actin focus that is short lived. The arrow points to a brightly staining region at a tricellular junction that remains bright throughout the time-lapse. The arrowhead points to a second such region, although in this case in the early time points it is slightly displaced from the tricellular junction. (G-L) *ap>actin-GFP* pupal wing a few hours later in development (~33 h awp). The time points are separated by 30 min. The red, blue and green arrows point to three cells where the bundle coalescence can be seen at this relatively late stage. (M-R) *ap>actin-GFP; mwh* pupal wings (~32 h awp). The green and red arrows follow actin bundles/hairs in two cells over the course of the time-lapse. Note the incomplete bundle fusion. The time points are separated by 30 min. (S-W) A different *ap>actin-GFP; mwh* pupal wing. The purple, red, green and blue arrows follow the formation of hairs/actin bundles that form at different times. In this cell the fusion of bundles is complete and the multiple hairs arise from successive rounds of initiation.

arrowheads). These are most commonly seen at tricellular junctions. We also see brightly staining puncta in the apical cortex (Fig. 2A-F). These are dynamic and are typically seen in only one image in a time-lapse series when images are taken every minute (Fig. 2A-F, asterisks; supplementary material Movie 1). Once hair initiation has occurred and outgrowth has begun, the growing hair often contains a number of distinct actin bundles (Fig. 2G-L, arrows; supplementary material Movie 2). On average, we detected 5.95 bundles per cell (Fig. 3) early in outgrowth. As outgrowth continues these fuse, leading to each cell forming a single hair (Fig. 2G-L, arrows; supplementary material Movie 2). The coalescence typically takes place over a period of ~2-3 h.

In these preparations we could not determine whether the multiple actin bundles seen in most cells were within a single hair or represented multiple hairs, each of which was covered by a separate region of plasma membrane. To distinguish between these two possibilities we also imaged pupal wings in which the plasma membrane was labeled with GFP (ap-Gal4>MCD8-GFP). In such wings we often observed cells with two hairs and also cells with a single irregularly shaped hair. The hairs took on their normal appearance as development proceeded. We further imaged *sqh-cherry-moesin;* ap>MCD8-GFP pupal wings. The Cherry-Moesin signal is rather weak but in mid-stage wings we were able to image the actin cytoskeleton in hairs and could see that there were often multiple hairs outlined by MCD8-GFP staining and filled with actin labeled by Cherry-Moesin (supplementary material Fig. S3). Thus, we are confident that the multiple bundles of actin-GFP observed in otherwise wild-type cells represent multiple hairs, each of which is covered by its own segment of plasma membrane. We cannot rule out that, at very early stages when the Cherry-Moesin reporter was too faint to be useful, discrete multiple bundles are present within a single hair.

In both the fixed wings and in the *in vivo* imaging experiments we could sometimes observe cells where substantial hair outgrowth had not yet taken place but in which there was a clear increase in F-actin in the vicinity of the distal vertex (supplementary material Fig. S4). We previously found in fixed wild-type wing cells that this area comprised 8.7±0.02% (s.d.) of the apical surface (Lu and Adler, 2015), and in our *in vivo* imaging experiments it comprised 7.2±0.03% (supplementary material Fig. S4A-C,G). This difference was not significant (*t*-test, P=0.06). We consider this to be an estimate of the fraction of the apical surface in which the actin cytoskeleton is activated to drive hair outgrowth.

When we captured images of actin-GFP-labeled growing hairs that were overexposed we observed very thin projections from the distal tips of hairs that contained actin (supplementary material Fig. S5B, arrows). We have not seen such structures in fixed and phalloidin-stained wings, suggesting that these projections are not stable to the fixation/staining procedures. Such projections were seen without overexposure when we used MCD8-GFP as a reporter (supplementary material Fig. S5A, arrows). In several instances, we also saw a 'blob' at the distal tip of the hair. We previously observed blob-like extensions during *in vivo* imaging using Rab11-GFP as a reporter for hairs (Nagaraj and Adler, 2012). That we were able to see these using very different types of reporter (actin and membrane) indicates that they are unlikely to be artifactual, although their functional importance is unclear.

Hair development in *mwh* mutants

We stained fixed *mwh* wings of various ages for F-actin (Fig. 1I-L). Prior to hair initiation we observed ectopic actin filaments and foci (Fig. 1I, arrows). Around the time of hair initiation we observed small foci of bright F-actin staining and apparent bundles of F-actin. In general, the F-actin organization of *mwh* cells appeared disorganized compared with that of wild-type cells. Hair formation was spread over a larger region than in wild type and many more hairs were formed (Fig. 1J-K, arrowheads). Some of the hairs were very short (Fig. 1G,H) and this phenotype is a striking characteristic of *mwh* mutants not seen in other PCP mutants.

In vivo imaging of the actin cytoskeleton in *mwh* mutant wings revealed several differences from wild type. Hair initiation often occurred over a larger part of the cell periphery and not just in the vicinity of the distal vertex as in wild type (Fig. 2M, arrows;

Development (2015) 142, 2478-2486 doi:10.1242/dev.122119

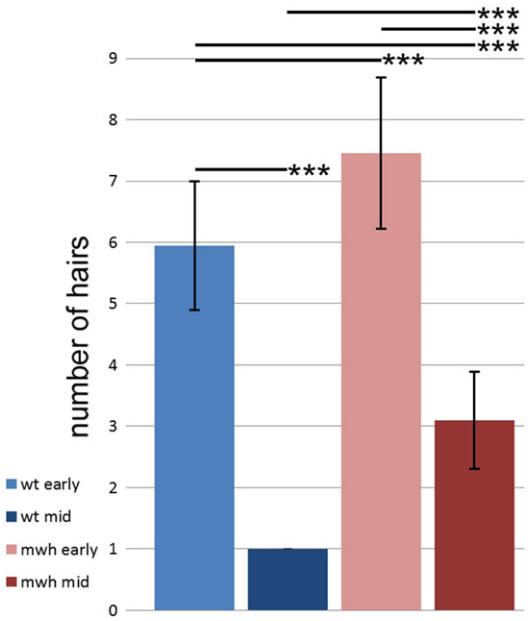

Fig. 3. Quantitation of the Mwh phenotype. The coalescence of hairs is incomplete in *mwh* mutants. The average number of hairs/actin bundles per cell is compared for *ap>actin-GFP* and *ap>actin-GFP; mwh* wings at both early (32 h) and middle (36 h) stages in development. Error bars are s.d.; 20 cells were scored for each point; ***P<0.001 (t-test).

supplementary material Fig. S4D-F,H and Movies 3 and 4). We routinely observed substantially more actin bundles and hairs (7.95 bundles/cell) than in wild type (Fig. 2M-W and Fig. 3), although the severity of the phenotype varied from one region of the wing to another (e.g. compare Fig. 2M-R with S-W), as is the case in the *mwh* adult wing. In the more severely affected regions it was not unusual to see as many as ten or more actin bundles in a single cell (e.g. Fig. 2N,O, red arrows). As development proceeded we observed fusion of bundles, but this did not proceed to completion as is seen in wild type (Fig. 2M-R and Fig. 3). During the growth of the primary hair(s) additional hairs continued to form (Fig. 2S-W, red, green and blue arrows; supplementary material Movie 4). These sometimes contained multiple actin bundles that fused, although in some cases the fusion was only partial and a split hair was seen (Fig. 2R). This delayed hair formation is presumably the source of the small hairs found on adult *mwh* wings (Fig. 1G,H) and confirms a suggestion made previously based on experiments with a temperature-sensitive allele of *mwh* (Yan et al., 2008). We also observed what might be bundle/hair fissions, although we could not rule out the possibility that these represented the formation of an additional bundle in the vicinity of an existing one.

In summary, our observations established that in the *mwh* mutant there were defects that led to multiple hair initiations over space and time and a failure in bundle fusion proceeding to completion. All three of these factors play a role in generating the MHC phenotype. If we assume that all of the short hairs are due to delayed formation and that the relatively long hairs are due to increased initial numbers and incomplete coalescence then we can estimate the relative contribution of the two mechanisms by counting the long and short hairs on adult wings. In two independent data sets obtained in this way, we found that delayed formation (short hairs) was responsible for slightly more than half (52.8% and 50.3%) of the hairs.

In both fixed *mwh* wings and in the *in vivo* imaging experiments we could sometimes observe cells where substantial hair outgrowth had not yet taken place but in which there was a clear increase in F-actin in the vicinity of the distal vertex. We measured this area as we had for wild-type cells (supplementary material Fig. S4D-F,H) and found that it increased from 8.7% in wild-type to 16±0.069% (s.d.) in *mwh* fixed cells. This difference was highly significant (t-test, P=0.0004). In the *in vivo* imaging experiments the area increased from 7.2% in wild type to 15±0.048% in *mwh*. Once again, the difference was highly significant (t-test, $P=1\times10^{-7}$). The difference between the fixed and live *mwh* cells was not significant (t-test, P=0.61). These data confirmed our conclusion from simple observation that the area over which the actin cytoskeleton is activated is increased in *mwh*.

Mwh-GBD-FH3 shows *in vivo* activity

Previously, we generated transgenic flies in which we could induce the expression of N- or C-terminal partial Mwh proteins (Yan et al., 2009). No gain-of-function phenotype was seen when either of these was expressed. Recently, we realized that expression of the N-terminal fragment (Mwh-GBD-FH3) could provide partial rescue of the mwh^1 mutant phenotype (Fig. 4A-C; supplementary material Fig. S6). By contrast, the C-terminal fragment did not show any rescue activity. Thus, although the Mwh-GBD-FH3 fragment (amino acids 60-491) only comprises ~50% of the wild-type protein (431 out of 836 amino acids), remarkably it retains substantial Mwh activity. Not surprisingly, this is the most conserved region of Mwh (supplementary material Table S1). In addition to partial rescue of the wing hair phenotype we also observed substantial rescue of the *mwh* arista phenotype (Fig. 4D-G) (He and Adler, 2002). The activity of the Mwh-GBD-FH3 fragment proved to be important for the *in vitro* analysis of Mwh function as we were unable to purify soluble full-length Mwh whereas we were able to purify Mwh-GBD-FH3 (supplementary material Fig. S7).

Mwh-GBD-FH3 can inhibit actin polymerization and crosslink, bundle and network actin filaments

As a first test of the effect of the GBD-FH3 fragment of Mwh on actin filaments we monitored the assembly of pyrenyl-actin. Mwh-GBD-FH3 potently inhibited assembly of G-actin and decreased actin polymerization induced by spectrin-F-actin seeds in a dose-dependent manner (Fig. 5A). However, once equilibrium was achieved (e.g. overnight versus 20 min incubation) the amount of F-actin was not reduced by Mwh-GBD-FH3 (supplementary material Fig. S8). We conclude that Mwh-GBD-FH3 slowed the rate of actin addition to existing filaments. These results raised the possibility that the ability to inhibit actin polymerization is a conserved feature of GBD-FH3 domains. To test this we purified Dia-GBD-FH3 protein and tested it for possible effects on actin polymerization (supplementary material Figs S7 and S9). Unlike Mwh-GBD-FH3, Dia-GBD-FH3 did not act as a potent inhibitor of actin polymerization. Thus, inhibition by GBD-FH3 is presumably a selective feature of Mwh and not a conserved feature of GBD-FH3 domains.

As an independent test of the effects of Mwh-GBD-FH3 on actin filaments we used total internal reflection fluorescence (TIRF) microscopy to observe the elongation of individual filaments. Mwh-GBD-FH3 at 50 nM had no effect on filament elongation, but at 100 nM the rate of filament elongation was significantly reduced (supplementary material Fig. S10). Thus, by two independent assays Mwh-GBD-FH3 decreased the rate of actin polymerization. We note that the results with 50 nM Mwh-GBD-FH3 were different in the pyrene and TIRF assembly assays. The reason for this is not

Development (2015) 142, 2478-2486 doi:10.1242/dev.122119

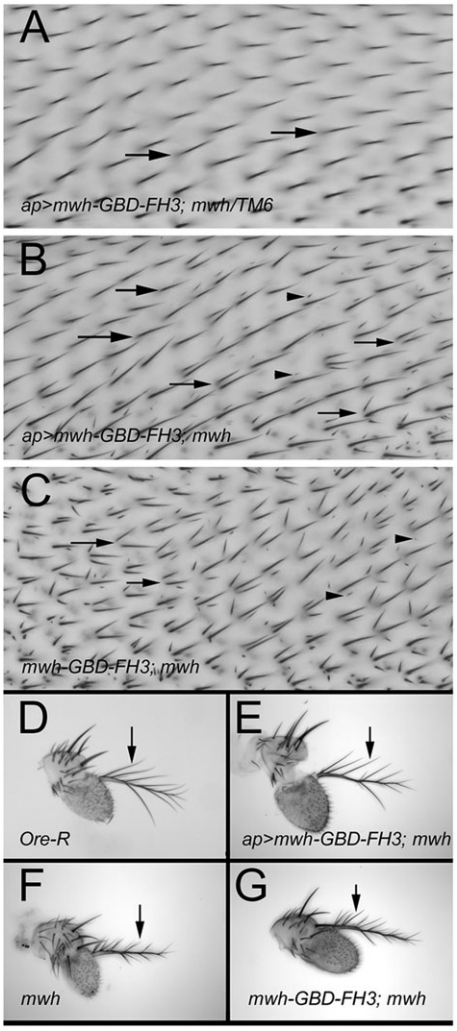

Fig. 4. The Mwh-GBD-FH3 fragment shows substantial rescue activity. The *ap>mwh-GBD-FH3; mwh*/*TM6* wing has a wild-type phenotype (A), whereas a strong *mwh* mutant phenotype is seen in *mwh-GBD-FH3; mwh* siblings (C). Note the substantial rescue of this mutant phenotype in *ap>mwh-GBD-FH3; mwh* sibling wings (B). The large arrows point to cells that formed a single hair, the small arrows to cells that formed two or more relatively normal length hairs, and the arrowheads to the very short hairs that are typical of *mwh*. (D-G) Rescue of the *mwh* arista phenotype. The arrows point to the long lateral projections formed on the arista. Compared with wild-type (D), these are short, split and multiple in *mwh* mutants (F,G), and note how this phenotype is largely rescued by the expression of Mwh-GBD-FH3 (E).

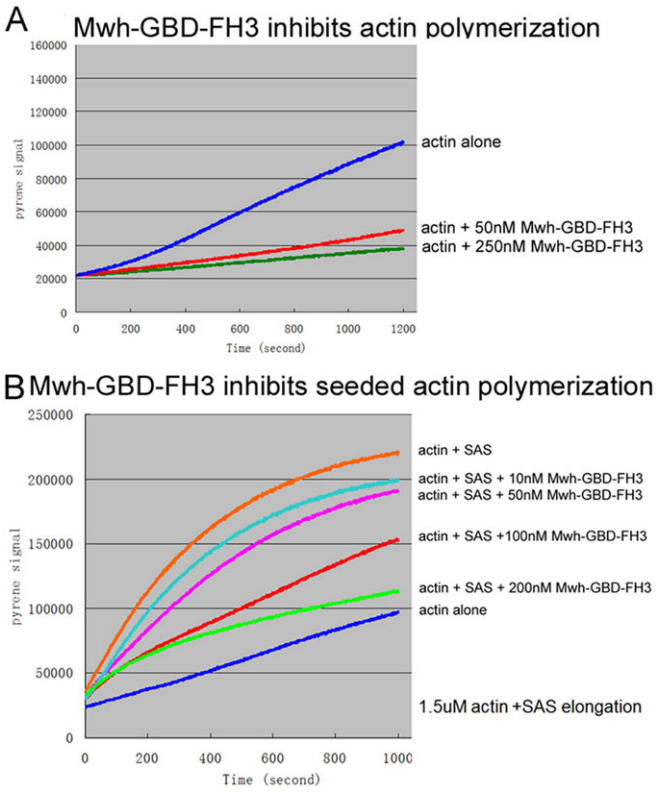

Fig. 5. Mwh-GBD-FH3 inhibits actin assembly *in vitro*. A pyrene actin assembly assay shows a dose-sensitive inhibition by purified Mwh-GBD-FH3 (A) (supplementary material Fig. S10). This is also seen when actin seeds are added (B), indicating that Mwh-GBD-FH3 inhibits the elongation of filaments.

clear but it could be due to the bundling activity (see below) differentially affecting polymerization in the two assays.

The ability of Mwh-GBD-FH3 to inhibit actin elongation could be mediated by its binding to either actin monomers or filaments. To determine if Mwh-GBD-FH3 bound actin filaments we used high-speed centrifugation. Mwh-GBD-FH3 associated with F-actin sedimented in the pellet fractions but was not detected with monomeric actin in the supernatant fractions (Fig. 6A). We were unable to saturate the binding of Mwh-his$_6$-GBD-FH3 to F-actin even when the molar ratio of Mwh-GBD-FH3 to actin was 2:3. This suggests that Mwh-GBD-FH3 is likely to bind to the side, rather than to the ends, of filaments.

Since Mwh is implicated in the coalescence of F-actin in developing hairs of the fly wing, we next tested if it could bundle actin filaments using a low-speed F-actin pelleting assay. Bundled actin filaments sediment at low speed, whereas individual actin filaments do not. As expected, in reactions containing 3 µM actin, little actin was found in the low-speed pellet fraction (Fig. 6B). However, in the presence of 500 nM Mwh-GBD-FH3, a large amount of actin was recovered in the low-speed pellet fraction (Fig. 6B). This indicated that Mwh-GBD-FH3 binds to actin filaments and crosslinks them as bundles.

We confirmed that Mwh-GBD-FH3 bundled actin filaments using TIRF microscopy (Fig. 7). Bundled filaments, which were identified as bright, linear structures scattered in the microscope field, formed in the presence of 150 nM Mwh-GBD-FH3 (Fig. 7C); higher concentrations of Mwh-GBD-FH3 (300 and 400 nM) resulted in the formation of shorter bundled arrays, among fewer actin filaments (Fig. 7D), consistent with its negative effects on actin polymerization. A variety of morphologies were seen among the bundled filaments. Examples from time-lapse images are shown in supplementary material Fig. S11. Filament bundles were rarely, if ever, observed in samples containing actin alone or actin and an unrelated 6×His-tagged CD44 protein (Fig. 7B).

The ability of Mwh-GBD-FH3 to bundle F-actin suggested that it acts as a dimer (or higher multimer) containing multiple binding sites. We attempted to determine whether Mwh and/or Mwh-GBD-FH3 could form dimers using the yeast two-hybrid system and by co-immunoprecipitation experiments. We obtained a relatively strong positive interaction between full-length Mwh and Mwh-GBD-FH3 in the yeast two-hybrid system (supplementary material Fig. S12) suggesting that these proteins could form dimers. We could also pull down full-length Mwh using anti-HA antibody on extracts of cells that expressed both Mwh-GBD-FH3-3HA and

Development (2015) 142, 2478-2486 doi:10.1242/dev.122119

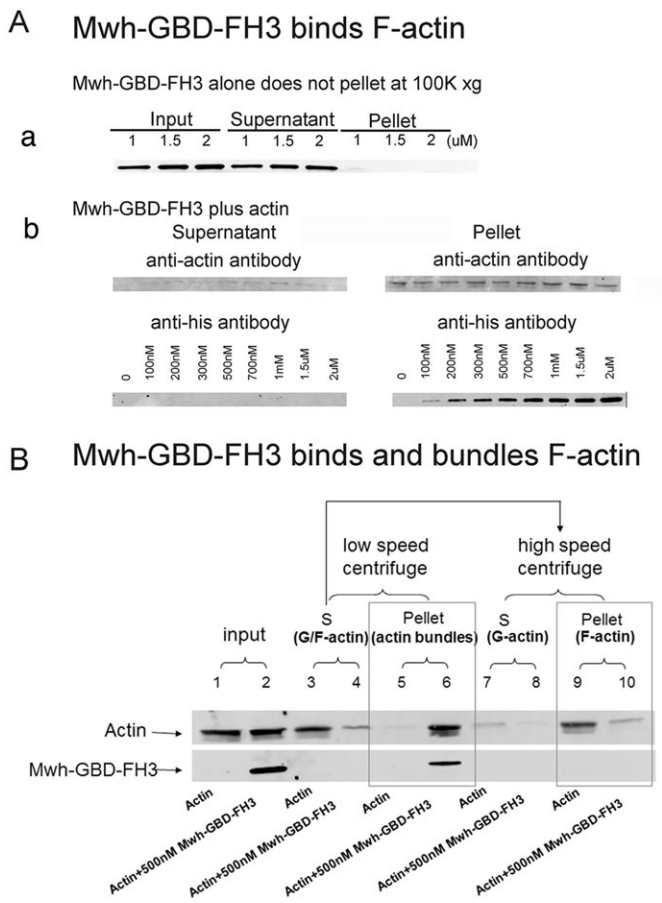

Fig. 6. Mwh-GBD-FH3 binds to and bundles F-actin. (A) Mwh-his$_6$-GBD-FH3 at a high concentration was not pelleted by centrifugation at 100,000 ***g*** (a) but, when mixed with 3 µM actin, it was found in the F-actin pellet at all the concentrations tested (b). This indicates that Mwh-his$_6$-GBD-FH3 binds to F-actin. Since the binding could not be saturated, it is likely to bind to the sides and not the ends of the filaments. (B) Assessment of actin filament bundling by Mwh-his$_6$-GBD-FH3 using low-speed centrifugation (10,000 ***g***). F-actin (3 µM) incubated alone did not pellet with low-speed centrifugation but, when mixed with Mwh-his$_6$-GBD-FH3, both proteins were found in the low-speed pellet. This indicates that the actin filaments and Mwh-GBD-FH3 formed a large bundled network.

Mwh (supplementary material Fig. S12). However, only a small amount of Mwh was pulled down in this experiment, suggesting that the interaction was weak.

DISCUSSION

Hair morphogenesis and PCP

The *fz/stan* pathway regulates PCP in the wing and other regions of the epidermis. Previous results established that this was accomplished by limiting the activation of the cytoskeleton that drives hair growth to the distalmost part of wing cells. Our *in vivo* imaging showed that hair morphogenesis is more complicated than previously appreciated. At early stages in hair growth multiple actin bundles and hairs form and then fuse to form a single distally pointing hair. We observed several abnormalities in *mwh* mutant wings. The area where actin polymerization (and hair initiation) occurred was increased and not restricted to the region around the distal vertex. The number of actin bundles at early times was increased and the fusion of bundles/hairs did not proceed to completion as in wild type. Furthermore, actin bundle formation and hair initiation continued well beyond the normal

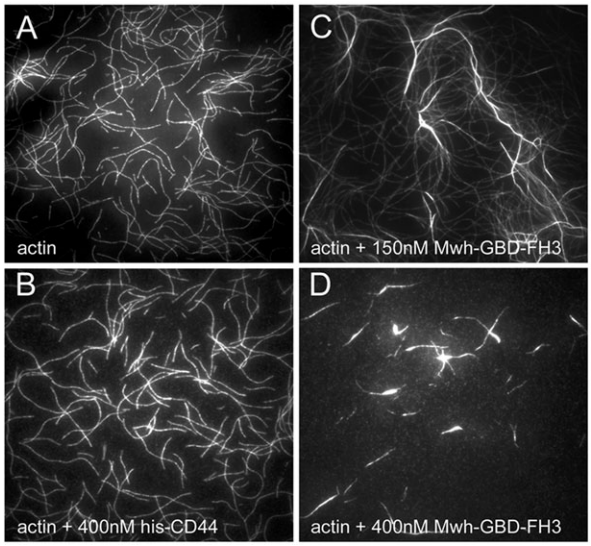

Fig. 7. Mwh-GBD-FH3 bundles F-actin. Shown are TIRF micrographs of labeled actin with (C,D) and without (A,B) incubation with Mwh-GBD-FH3. Note that 150 nM Mwh-GBD-FH3 resulted in bundled F-actin (C) and this was greatly enhanced at 400 nM Mwh-GBD-FH3 (D), although here the bundles were shorter and between fewer actin filaments owing to apparent negative effects of higher Mwh-GBD-FH3 concentrations on actin polymerization. The bundling was not due to the presence of the 6×His tag used in protein purification as the presence of 400 nM His$_6$-CD44 had no effect (B) compared with actin alone (A).

period. All of these factors contributed to the extreme multiple hair phenotype.

Mwh-GBD-FH3 inhibits actin polymerization and bundles actin filaments

The *in vivo* rescue activity of an N-terminal fragment of Mwh established the importance of the Mwh-GBD-FH3 domain for specifying the morphologies of F-actin-rich structures. Using purified Mwh-GBD-FH3 protein we identified two biochemical activities that correspond to the two activities of Mwh identified in genetic studies. Mwh-GBD-FH3 inhibited actin polymerization via effects on the rate of filament elongation and it crosslinked actin filaments as bundles. It is possible that the crosslinking activity contributes in some way to the inhibition of actin assembly. It is worth noting that Mwh is unlikely to be a general regulator of the actin cytoskeleton *in vivo*, but is likely to provide specialized PCP functions. *mwh* mutations do not result in phenotypes in most cell types, unlike well-characterized general regulators of the actin cytoskeleton such as *tsr* (cofilin) (Gunsalus et al., 1995), *flare* (AIP1) (Ren et al., 2007) and *dia* (Castrillon and Wasserman, 1994). Rather, Mwh appears to only function in the epidermis during the morphogenesis of cellular extensions whose polarity is under the control of the *fz/stan* pathway. It is somewhat surprising that a special actin regulator has evolved that appears to function only in the epidermis of *Drosophila* (and presumably other insects) to regulate the morphogenesis of cellular extensions. Why evolution selected for this solution, as opposed to modulating the activity of a general actin regulator, can only be speculated upon. It remains to be determined how common this strategy is. Based on what is known about protein domains that can directly bind to and modulate the actin cytoskeleton, one would not have predicted that Mwh-GBD-FH3 would be able to do so. Our finding that Mwh-GBD-FH3 does bind actin raises the possibility that there are as yet

Development (2015) 142, 2478-2486 doi:10.1242/dev.122119

undiscovered proteins and protein domains that function as potent actin regulators.

Our observation that the Mwh-GBD-FH3 domain inhibits actin polymerization, binds to and bundles actin filaments was surprising. GBD-FH3 domains in other proteins such as Dia have not been implicated in such activities and this region is thought to mediate regulation of the FH1 and FH2 domains. Indeed, the purified Dia GBD-FH3 fragment had no effects on actin polymerization *in vitro*. It is worth noting that the Mwh-GBD-FH3 domain, although recognizable, is more diverged than most such domains (Strutt and Warrington, 2008; Yan et al., 2008). The GBD in other proteins is known to bind Rho-GTP; consistent with this role, Rho1 and Mwh-GBD-FH3 co-immunoprecipitate (Yan et al., 2009). The ability of Mwh-GBD-FH3 to directly bind actin presumably does not require activation by Rho1-GTP, as Rho1 was not present in our *in vitro* experiments. However, Rho1-GTP might be required for F-actin binding by full-length Mwh protein.

The role of Mwh during wing development

Prior to hair initiation Mwh is found preferentially on the proximal side of wing cells far from where the actin cytoskeleton is activated to form the hair (Strutt and Warrington, 2008; Yan et al., 2008). We suggest that proximal Mwh locally inhibits the actin cytoskeleton to restrict hair formation to the distalmost part of the cell. Its proximal location is thought to be mediated by binding to the PPE protein Inturned (Lu et al., 2010). The PPE proteins as a group are recruited to the proximal side of wing cells as instructed by the upstream PCP proteins (Adler et al., 2004; Strutt and Warrington, 2008; Wang et al., 2014). This cascade of regulatory complexes provides a mechanism to transduce the PCP signal to the cytoskeleton.

During hair elongation Mwh is found in the growing hair and later preferentially accumulates at the base of the hair (Yan et al., 2008). Our *in vivo* imaging of wild-type wings suggested that the coalescence of actin bundles is important for normal hair morphogenesis. Imaging of *mwh* mutant wings established that bundle/hair fusion was not complete. Since Mwh-GBD-FH3 bundled actin filaments *in vitro*, we suggest that the bundling activity is likely to be important for the coalescence of actin bundles, insuring that only a single hair is formed.

Temperature-shift experiments with a temperature-sensitive *mwh* allele inferred that *mwh* functions at two times during hair morphogenesis (Yan et al., 2008). Prior to hair morphogenesis it is required to restrict hair initiation to the distalmost region of wing cells and through this mechanism it ensures distal polarity. A second function is presumed to be in inhibiting ectopic hair formation after the normal time of hair initiation. The key observation here was that a shift from the permissive to restrictive temperature a couple of hours after hair initiation resulted in cells forming a single, long, distally pointing hair (due to normal early function) as well as one or several very small hairs. These very small hairs are also seen in *mwh* null mutants. Our *in vivo* imaging showed the formation of such small ectopic hairs several hours after the original phase of hair initiation, establishing that our previous hypothesis was correct.

MATERIALS AND METHODS

Fly genetics

All flies were raised at 25°C unless otherwise stated. Mutant fly lines, reporter lines and Gal4 stocks were obtained from the Bloomington *Drosophila* Stock Center. The *UAS-mwh* lines were generated previously in this laboratory (Yan et al., 2008, 2009). To direct transgene expression, we used the Gal4/UAS system (Brand and Perrimon, 1993). For immunostaining, white pupae were collected and grown at 25°C for 30, 32, 35 or 36 h before fixation.

Analysis of adult wing phenotypes

Adult wings were dehydrated in 100% ethanol and then mounted in Euparal (ASCO Laboratories). Mounted samples were examined under the bright-field microscope.

Gene manipulations

Two differently tagged *UAS-mwh-GBD-FH3* constructs were made. The *UAS-GBD-FH3-3HA* construct was made by PCR using cDNA of *mwh* encoding the GBD-FH3 domain with Gateway cassette sequences (Invitrogen) on both sides. The primers are: 5′-GGGGACAAGTTTGTACAAAAAAGCAGGCTTCCAAAACATGTACAGCAAGGAAAACCAGCG-3′ and 5′-GGGGACCACTTTGTACAAGAAAGCTGGGTCGATGCCCTCGTCCTCGTG-3′. The cDNA was cloned into Donor 221 vector (Invitrogen) to generate the entry clone, which was then cloned into pTWH Gateway vector (Invitrogen) to generate an expression construct with a C-terminal 3HA tag.

The *UAS-GBD-FH3-GFP* construct was made using a similar strategy but substituting the pTWG Gateway vector (Invitrogen) to generate a construct with a C-terminal GFP tag.

Protein purification

To prepare recombinant Mwh-GBD-FH3 cDNA, sequences that encoded amino acids 60-491 were subcloned into PET28A (Invitrogen). The vector provides a His_6 tag on the N-terminus of the protein. Expression was induced by IPTG and pelleted bacteria were lysed by sonication. The protein was present in inclusion bodies that were recovered by centrifugation, washed three times, solubilized in 50 mM Tris-HCl (pH 8.0), 500 mM NaCl, 8 M urea, and the urea then removed by dialysis. The protein was then purified by affinity chromatography on Ni-NTA columns (Life Technologies) and molecular size-exclusion chromatography. Actin was prepared from chicken pectoral muscle and gel filtered as described (Spudich and Watt, 1971). Pyrenyl-actin was prepared as described (Bryan and Coluccio, 1985). Spectrin F-actin seeds (SAS) were prepared as described (DiNubile et al., 1995).

In vitro actin polymerization

Actin assembly reactions contained 1-4 µM actin (10% pyrene labeled) and either Mwh-GBD-FH3 or Dia-FH1-FH2, as indicated, in 20 mM imidazole (pH 7.0), 50 mM KCl, 2 mM $MgCl_2$, 1 mM EGTA (MKEI-50 buffer), 0.2 mM ATP and 0.1 mM DTT. Spectrin F-actin seeds (0.2 nM) were included in seeded assembly assays. G-actin was treated with 0.1 mM $MgCl_2$ and 1 mM EGTA for 60 s prior to starting the assembly reaction. Fluorescence of pyrenyl-actin (excitation at 365 nm, emission at 386 nm) was monitored over time at 25°C using a QuantaMaster spectrofluorometer (PTI).

Analysis of actin filament binding and bundling

Different concentrations of Mwh-his_6-GBD-FH3 were incubated with 3 µM actin in MKEI-50 buffer overnight at 25°C. Control reactions contained actin or Mwh-his_6-GBD-FH3 alone. Reactions were centrifuged at 70,000 rpm (100,000 ***g***) for 20 min at 4°C in a TLA-120.2 rotor (Beckman Coulter), and samples of supernatant fractions and F-actin were analyzed on 4-20% SDS-PAGE gels (Invitrogen) followed by transfer to nitrocellulose. Actin was detected on blots using anti-actin monoclonal antibody (C4; Abcam, ab3280; 1:1000); anti-His (Invitrogen, 37-2900; 1:500) was used to detect Mwh-his_6-GBD-FH3.

Low-speed (17,000 rpm, 10,000 ***g***) pelleting assays of Mwh-GBD-FH3 were performed similarly as described for the high-speed pelleting assays.

Total internal reflection fluorescence (TIRF) microscopy

Glass coverslips were cleaned, silanized, assembled into chambers and blocked by two washes with 1% BSA in 50 mM Tris-Cl (pH 7.6), 50 mM NaCl and twice with MKEI-50 buffer (Kuhn and Pollard, 2005). To prevent non-specific binding of Mwh-GBD-FH3 proteins, the chambers were blocked with 5% F-127 pluronic acid followed by two washes with 1% BSA-containing buffer and twice with MKEI-50 buffer. TIRF microscopy was performed using an Olympus X71 inverted microscope equipped for through-the-lens TIRF using an argon laser and a 1.45 N.A. objective lens in combination with a 1.5× auxiliary lens. Image acquisition began 30-60 s after flowing the sample into the chamber. Images (0.5 s exposure) were collected

at 3- or 5-s intervals for up to 10 min on an Orca-Flash 4.0 CMOS camera (Hamamatsu) controlled by MetaMorph software (Molecular Devices).

Actin assembly assay under TIRF microscopy

1 µM actin (8% Alexa 488-actin) was primed for 1 min with 1/8 volume of 0.8 mM EGTA, 0.08 mM $MgCl_2$ and added to imaging buffer [10 mM imidazole (pH 7.0), 100 mM KCl, 1 mM $MgCl_2$, 1 mM EGTA, 0.3% methylcellulose, 40 mM DTT, 80 µg/ml glucose oxidase, 40 µg/ml catalase, 3 mg/ml glucose and 0.2 mM ATP]. The reaction proceeded for 1 min, and a 10 µl aliquot was flowed into a chamber and incubated for an additional 2 min. A second reaction containing 1 µM actin (8% Alexa 488-actin) primed as described above was mixed with imaging buffer containing 0.4% methylcellulose with different concentrations of Mwh-GBD-FH3. A 10 µl aliquot was flowed into the same chamber as above. Images were collected at a rate of one frame every 5 s for 120 frames. Filament growth rates were determined for ten filaments by manually measuring filament lengths in ImageJ (NIH). Only attached filaments were tracked. A fiducial mark (speckle or the start point) on the filament was used as a reference point at the barbed end. The rate of growth of each filament was calculated based on the difference in length to the reference point over 24 frames in the first 5 min. Rates were compared using two-sample unequal variance Student's *t*-test in Microsoft Excel. As a control for possible effects of the His tag present on Mwh-GBD-FH3 we tested the effects of His-CD44 recombinant human protein in actin assembly reactions.

In vivo imaging of hair formation

Pupae were dissected out of the pupal case and placed in a microscope chamber made using double-sided sticky tape and silicone spacers. A small amount of Halocarbon oil was used to create a good optical interface between the pupa and the cover slip. A small piece of moist filter paper was inserted below the cover slip to prevent dehydration of the pupa. Imaging was performed on a Zeiss 780 confocal microscope with 63× oil objective. Images were taken every 15 min with optical sections every 0.2 µm. *ap>UAS-actin-GFP*, *ap>UAS-lifeact-GFP* and *sqh-moe-cherry* were used for imaging the actin cytoskeleton.

Acknowledgements

We thank our colleagues in the fly community for generously sharing reagents. Special thanks to FlyBase and the Bloomington and Vienna stock centers. We thank the Keck Center for Cellular Imaging where many of the experiments were carried out.

Competing interests

The authors declare no competing or financial interests.

Author contributions

P.N.A. conceived and directed the project. D.A.S. directed the *in vitro* actin assays. Q.L. carried out most of the experiments. P.N.A. carried out some of the genetic experiments. All of the authors contributed in designing experiments and analyzing the data. P.N.A. wrote the manuscript and both Q.L. and D.A.S. helped in revising it. Q.L. prepared the initial version of the figures and P.N.A. revised them.

Funding

This work was supported by a grant from the National Institutes of Health [GM037163] to P.N.A. Deposited in PMC for release after 12 months.

Supplementary material

Supplementary material available online at http://dev.biologists.org/lookup/suppl/doi:10.1242/dev.122119/-/DC1

References

Adler, P. N. (1992). The genetic control of tissue polarity in Drosophila. *Bioessays* **14**, 735-741.
Adler, P. N. (2002). Planar signaling and morphogenesis in Drosophila. *Dev. Cell* **2**, 525-535.
Adler, P. N., Charlton, J. and Liu, J. (1998). Mutations in the cadherin superfamily member gene dachsous cause a tissue polarity phenotype by altering frizzled signaling. *Development* **125**, 959-968.
Adler, P. N., Zhu, C. M. and Stone, D. (2004). Inturned localizes to the proximal side of wing cells under the instruction of upstream planar polarity proteins. *Curr. Biol.* **14**, 2046-2051.
Alberts, A. S. (2001). Identification of a carboxy-terminal diaphanous-related formin homology protein autoregulatory domain. *J. Biol. Chem.* **276**, 2824-2830.
Axelrod, J. D. (2001). Unipolar membrane association of dishevelled mediates frizzled planar cell polarity signaling. *Genes Dev.* **15**, 1182-1187.
Bastock, R., Strutt, H. and Strutt, D. (2003). Strabismus is asymmetrically localised and binds to Prickle and Dishevelled during Drosophila planar polarity patterning. *Development* **130**, 3007-3014.
Brand, A. H. and Perrimon, N. (1993). Targetted gene expression as a means of altering cell fate and generating dominant phenotypes. *Development* **118**, 401-415.
Breitsprecher, D. and Goode, B. L. (2013). Formins at a glance. *J. Cell Sci.* **126**, 1-7.
Bryan, J. and Coluccio, L. M. (1985). Kinetic analysis of F-actin depolymerization in the presence of platelet gelsolin and gelsolin-actin complexes. *J. Cell Biol.* **101**, 1236-1244.
Campellone, K. G. and Welch, M. D. (2010). A nucleator arms race: cellular control of actin assembly. *Nat. Rev. Mol. Cell Biol.* **11**, 237-251.
Casal, J., Lawrence, P. A. and Struhl, G. (2006). Two separate molecular systems, Dachsous/Fat and Starry night/Frizzled, act independently to confer planar cell polarity. *Development* **133**, 4561-4572.
Castrillon, D. H. and Wasserman, S. A. (1994). Diaphanous is required for cytokinesis in Drosophila and shares domains of similarity with the products of the limb deformity gene. *Development* **120**, 3367-3377.
Chang, H. and Nathans, J. (2013). Responses of hair follicle-associated structures to loss of planar cell polarity signaling. *Proc. Natl. Acad. Sci. USA* **110**, E908-E917.
Chin, M.-L. and Mlodzik, M. (2013). The Drosophila selectin furrowed mediates intercellular planar cell polarity interactions via frizzled stabilization. *Dev. Cell* **26**, 455-468.
Das, G., Jenny, A., Klein, T. J., Eaton, S. and Mlodzik, M. (2004). Diego interacts with Prickle and Strabismus/Van Gogh to localize planar cell polarity complexes. *Development* **131**, 4467-4476.
DiNubile, M. J., Cassimeris, L., Joyce, M. and Zigmond, S. H. (1995). Actin filament barbed-end capping activity in neutrophil lysates: the role of capping protein-beta 2. *Mol. Biol. Cell* **6**, 1659-1671.
Eaton, S., Wepf, R. and Simons, K. (1996). Roles for Rac1 and Cdc42 in planar polarization and hair outgrowth in the wing of Drosophila. *J. Cell Biol.* **135**, 1277-1289.
Ezan, J. and Montcouquiol, M. (2013). Revisiting planar cell polarity in the inner ear. *Semin. Cell Dev. Biol.* **24**, 499-506.
Feiguin, F., Hannus, M., Mlodzik, M. and Eaton, S. (2001). The ankyrin repeat protein Diego mediates Frizzled-dependent planar polarization. *Dev. Cell* **1**, 93-101.
Franke, J. D., Montague, R. A. and Kiehart, D. P. (2010). Nonmuscle myosin II is required for cell proliferation, cell sheet adhesion and wing hair morphology during wing morphogenesis. *Dev. Biol.* **345**, 117-132.
Gho, M. and Schweisguth, F. (1998). Frizzled signalling controls orientation of asymmetric sense organ precursor cell divisions in Drosophila. *Nature* **393**, 178-181.
Goode, B. L. and Eck, M. J. (2007). Mechanism and function of formins in the control of actin assembly. *Annu. Rev. Biochem.* **76**, 593-627.
Goodrich, L. V. and Strutt, D. (2011). Principles of planar polarity in animal development. *Development* **138**, 1877-1892.
Goto, T. and Keller, R. (2002). The planar cell polarity gene strabismus regulates convergence and extension and neural fold closure in Xenopus. *Dev. Biol.* **247**, 165-181.
Gubb, D. and Garcia-Bellido, A. (1982). A genetic analysis of the determination of cuticular polarity during development in Drosophila melanogaster. *J. Embryol. Exp. Morphol.* **68**, 37-57.
Guild, G. M., Connelly, P. S., Ruggiero, L., Vranich, K. A. and Tilney, L. G. (2005). Actin filament bundles in Drosophila wing hairs: hairs and bristles use different strategies for assembly. *Mol. Biol. Cell* **16**, 3620-3631.
Gunsalus, K. C., Bonaccorsi, S., Williams, E., Verni, F., Gatti, M. and Goldberg, M. L. (1995). Mutations in twinstar, a Drosophila gene encoding a cofilin/ADF homologue, result in defects in centrosome migration and cytokinesis. *J. Cell Biol.* **131**, 1243-1259.
Harris, E. S., Li, F. and Higgs, H. N. (2004). The mouse formin, FRLalpha, slows actin filament barbed end elongation, competes with capping protein, accelerates polymerization from monomers, and severs filaments. *J. Biol. Chem.* **279**, 20076-20087.
Harris, E. S., Rouiller, I., Hanein, D. and Higgs, H. N. (2006). Mechanistic differences in actin bundling activity of two mammalian formins, FRL1 and mDia2. *J. Biol. Chem.* **281**, 14383-14392.
Harumoto, T., Ito, M., Shimada, Y., Kobayashi, T. J., Ueda, H. R., Lu, B. and Uemura, T. (2010). Atypical cadherins Dachsous and Fat control dynamics of noncentrosomal microtubules in planar cell polarity. *Dev. Cell* **19**, 389-401.
He, B. and Adler, P. N. (2002). The frizzled pathway regulates the development of arista laterals. *BMC Dev. Biol.* **2**, 7.
Heisenberg, C. P., Tada, M., Rauch, G. J., Saúde, L., Concha, M. L., Geisler, R., Stemple, D. L., Smith, J. C. and Wilson, S. W. (2000). Silberblick/Wnt11 mediates convergent extension movements during zebrafish gastrulation. *Nature* **405**, 76-81.

Held, L. I., Duarte, C. M. and Derakhshanian, K. (1986). Extra tarsal joints and abnormal cuticular polarities in various mutants of Drosophila melanogaster. *Roux's Arch. Dev. Biol.* **195**, 145-157.
Hermle, T., Guida, M. C., Beck, S., Helmstädter, S. and Simons, M. (2013). Drosophila ATP6AP2/VhaPRR functions both as a novel planar cell polarity core protein and a regulator of endosomal trafficking. *EMBO J.* **32**, 245-259.
Jessen, J. R., Topczewski, J., Bingham, S., Sepich, D. S., Marlow, F., Chandrasekhar, A. and Solnica-Krezel, L. (2002). Zebrafish trilobite identifies new roles for Strabismus in gastrulation and neuronal movements. *Nat. Cell Biol.* **4**, 610-615.
Kiehart, D. P., Franke, J. D., Chee, M. K., Montague, R. A., Chen, T.-L., Roote, J. and Ashburner, M. (2004). Drosophila crinkled, mutations of which disrupt morphogenesis and cause lethality, encodes fly myosin VIIA. *Genetics* **168**, 1337-1352.
Kitayama, C. and Uyeda, T. Q. P. (2003). ForC, a novel type of formin family protein lacking an FH1 domain, is involved in multicellular development in Dictyostelium discoideum. *J. Cell Sci.* **116**, 711-723.
Kuhn, J. R. and Pollard, T. D. (2005). Real-time measurements of actin filament polymerization by total internal reflection fluorescence microscopy. *Biophys. J.* **88**, 1387-1402.
Lawrence, P. A., Casal, J. and Struhl, G. (2004). Cell interactions and planar polarity in the abdominal epidermis of Drosophila. *Development* **131**, 4651-4664.
Lee, H. and Adler, P. N. (2002). The function of the frizzled pathway in the Drosophila wing is dependent on inturned and fuzzy. *Genetics* **160**, 1535-1547.
Li, F. and Higgs, H. N. (2005). Dissecting requirements for auto-inhibition of actin nucleation by the formin, mDia1. *J. Biol. Chem.* **280**, 6986-6992.
Lu, Q. and Adler, P. N. (2015). The diaphanous gene of Drosophila interacts antagonistically with multiple wing hairs and plays a key role in wing hair morphogenesis. *PLoS ONE* **10**, e0115623.
Lu, Q., Yan, J. and Adler, P. N. (2010). The Drosophila planar polarity proteins inturned and multiple wing hairs interact physically and function together. *Genetics* **185**, 549-558.
Ma, D., Yang, C.-h., McNeill, H., Simon, M. A. and Axelrod, J. D. (2003). Fidelity in planar cell polarity signalling. *Nature* **421**, 543-547.
Matis, M. and Axelrod, J. D. (2013). Regulation of PCP by the Fat signaling pathway. *Genes Dev.* **27**, 2207-2220.
Merkel, M., Sagner, A., Gruber, F. S., Etournay, R., Blasse, C., Myers, E., Eaton, S. and Jülicher, F. (2014). The balance of prickle/spiny-legs isoforms controls the amount of coupling between core and fat PCP systems. *Curr. Biol.* **24**, 2111-2123.
Montcouquiol, M., Rachel, R. A., Lanford, P. J., Copeland, N. G., Jenkins, N. A. and Kelley, M. W. (2003). Identification of Vangl2 and Scrb1 as planar polarity genes in mammals. *Nature* **423**, 173-177.
Moseley, J. B., Sagot, I., Manning, A. L., Xu, Y., Eck, M. J., Pellman, D. and Goode, B. L. (2004). A conserved mechanism for Bni1- and mDia1-induced actin assembly and dual regulation of Bni1 by Bud6 and profilin. *Mol. Biol. Cell* **15**, 896-907.
Nagaraj, R. and Adler, P. N. (2012). Dusky-like functions as a Rab11 effector for the deposition of cuticle during Drosophila bristle development. *Development* **139**, 906-916.
Olofsson, J., Sharp, K. A., Matis, M., Cho, B. and Axelrod, J. D. (2014). Prickle/spiny-legs isoforms control the polarity of the apical microtubule network in planar cell polarity. *Development* **141**, 2866-2874.
Petersen, N. S., Lankenau, D. H., Mitchell, H. K., Young, P. and Corces, V. G. (1994). forked proteins are components of fiber bundles present in developing bristles of Drosophila melanogaster. *Genetics* **136**, 173-182.
Ren, N., Charlton, J. and Adler, P. N. (2007). The flare gene, which encodes the AIP1 protein of Drosophila, functions to regulate F-actin disassembly in pupal epidermal cells. *Genetics* **176**, 2223-2234.
Shimada, Y., Yonemura, S., Ohkura, H., Strutt, D. and Uemura, T. (2006). Polarized transport of Frizzled along the planar microtubule arrays in Drosophila wing epithelium. *Dev. Cell* **10**, 209-222.
Spudich, J. A. and Watt, S. (1971). The regulation of rabbit skeletal muscle contraction. I. Biochemical studies of the interaction of the tropomyosin-troponin complex with actin and the proteolytic fragments of myosin. *J. Biol. Chem.* **246**, 4866-4871.
Strutt, D. (2001). Asymmetric localization of frizzled and the establishment of cell polarity in the Drosophila wing. *Mol. Cell* **7**, 367-375.
Strutt, D. and Warrington, S. J. (2008). Planar polarity genes in the Drosophila wing regulate the localisation of the FH3-domain protein Multiple Wing Hairs to control the site of hair production. *Development* **135**, 3103-3111.
Tada, M. and Smith, J. C. (2000). Xwnt11 is a target of Xenopus Brachyury: regulation of gastrulation movements via Dishevelled, but not through the canonical Wnt pathway. *Development* **127**, 2227-2238.
Tucker, J. B. (1981). Cytoskeletal coordination and intercellular signalling during metazoan embryogenesis. *J. Embryol. Exp. Morphol.* **65**, 1-25.
Turner, C. M. and Adler, P. N. (1998). Distinct roles for the actin and microtubule cytoskeletons in the morphogenesis of epidermal hairs during wing development in Drosophila. *Mech. Dev.* **70**, 181-192.
Usui, T., Shima, Y., Shimada, Y., Hirano, S., Burgess, R. W., Schwarz, T. L., Takeichi, M. and Uemura, T. (1999). Flamingo, a seven-pass transmembrane cadherin, regulates planar cell polarity under the control of frizzled. *Cell* **98**, 585-595.
Vinson, C. R. and Adler, P. N. (1987). Directional non-cell autonomy and the transmission of polarity information by the frizzled gene of Drosophila. *Nature* **329**, 549-551.
Vladar, E. K., Bayly, R. D., Sangoram, A. M., Scott, M. P. and Axelrod, J. D. (2012). Microtubules enable the planar cell polarity of airway cilia. *Curr. Biol.* **22**, 2203-2212.
Wallingford, J. B., Vogeli, K. M. and Harland, R. M. (2001). Regulation of convergent extension in Xenopus by Wnt5a and Frizzled-8 is independent of the canonical Wnt pathway. *Int. J. Dev. Biol.* **45**, 225-227.
Wang, Y. and Nathans, J. (2007). Tissue/planar cell polarity in vertebrates: new insights and new questions. *Development* **134**, 647-658.
Wang, J., Mark, S., Zhang, X., Qian, D., Yoo, S.-J., Radde-Gallwitz, K., Zhang, Y., Lin, X., Collazo, A., Wynshaw-Boris, A. et al. (2005). Regulation of polarized extension and planar cell polarity in the cochlea by the vertebrate PCP pathway. *Nat. Genet.* **37**, 980-985.
Wang, Y., Badea, T. and Nathans, J. (2006). Order from disorder: Self-organization in mammalian hair patterning. *Proc. Natl. Acad. Sci. USA* **103**, 19800-19805.
Wang, Y., Yan, J., Lee, H., Lu, Q. and Adler, P. N. (2014). The proteins encoded by the Drosophila planar polarity effector genes inturned, fuzzy and fritz interact physically and can re-pattern the accumulation of "upstream" planar cell polarity proteins. *Dev. Biol.* **394**, 156-169.
Winter, C. G., Wang, B., Ballew, A., Royou, A., Karess, R., Axelrod, J. D. and Luo, L. (2001). Drosophila rho-associated kinase (drok) links frizzled-mediated planar cell polarity signaling to the actin cytoskeleton. *Cell* **105**, 81-91.
Wong, L. L. and Adler, P. N. (1993). Tissue polarity genes of Drosophila regulate the subcellular location for prehair initiation in pupal wing cells. *J. Cell Biol.* **123**, 209-221.
Yan, J., Huen, D., Morely, T., Johnson, G., Gubb, D., Roote, J. and Adler, P. N. (2008). The multiple-wing-hairs gene encodes a novel GBD-FH3 domain-containing protein that functions both prior to and after wing hair initiation. *Genetics* **180**, 219-228.
Yan, J., Lu, Q., Fang, X. and Adler, P. N. (2009). Rho1 has multiple functions in Drosophila wing planar polarity. *Dev. Biol.* **333**, 186-199.
Yang, C.-h., Axelrod, J. D. and Simon, M. A. (2002). Regulation of Frizzled by fat-like cadherins during planar polarity signaling in the Drosophila compound eye. *Cell* **108**, 675-688.
Zheng, L., Zhang, J. and Carthew, R. W. (1995). frizzled regulates mirror-symmetric pattern formation in the Drosophila eye. *Development* **121**, 3045-3055.

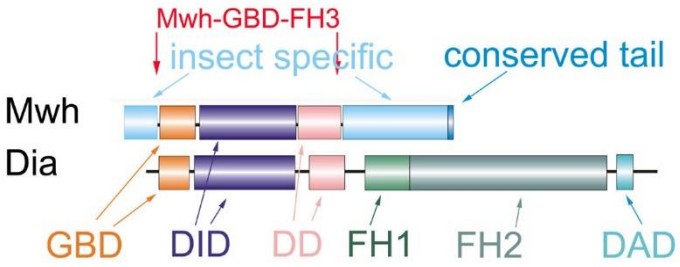

Figure S1. The domain structures of Dia and Mwh. Three domains in the amino terminal half of both Mwh and Dia are conserved. The FH1, FH2 and DAD located in the carboxy terminal half of Dia are not found in Mwh. Additionally, there are two regions of insect specific sequences as well as a short highly conserved insect specific C terminal region in Mwh that are not found in Dia. The Mwh-GBD-FH3 fragment is comprised of the GBD-DID-DD regions.

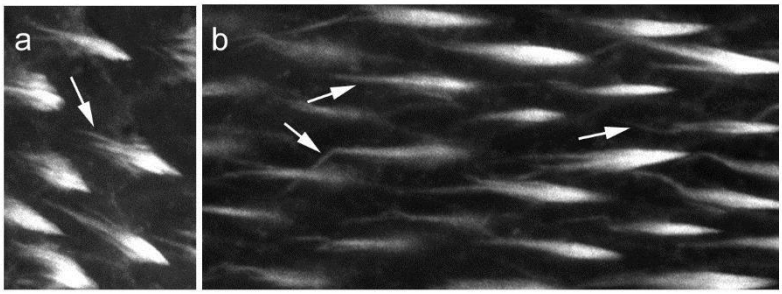

Figure S2. Growing hairs contain rootlets that extend proximally and basally. Both panels show wild type pupal wings. A is of a phalloidin stained Oregon-R wing and B of a live *ap>actin-GFP* pupal wing. The arrows point to the rootlets.

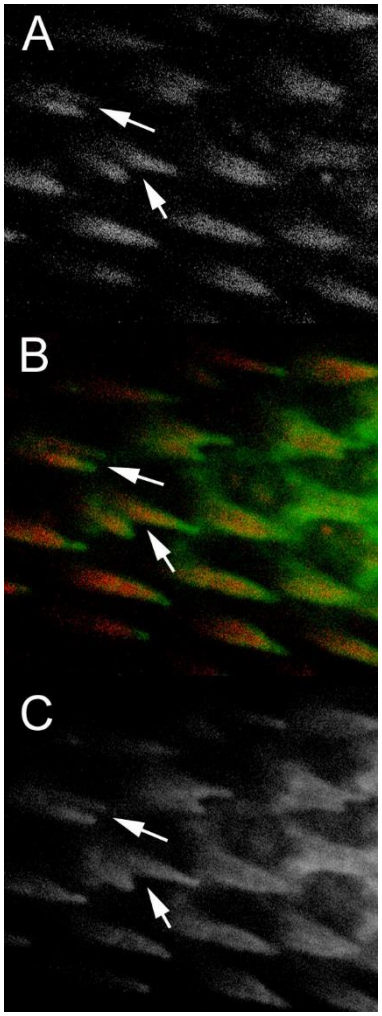

Figure S3. Dual imaging of actin and the plasma membrane during hair outgrowth. *ap>UAS-MCD8-GFP, ap>moe-cherry* pupal wings were imaged in living pupae. The arrows point to cells that have formed multipled or split hairs. This is visible with both reporters hence the multiple hairs are each enclosed by their own section of plasma membrane.

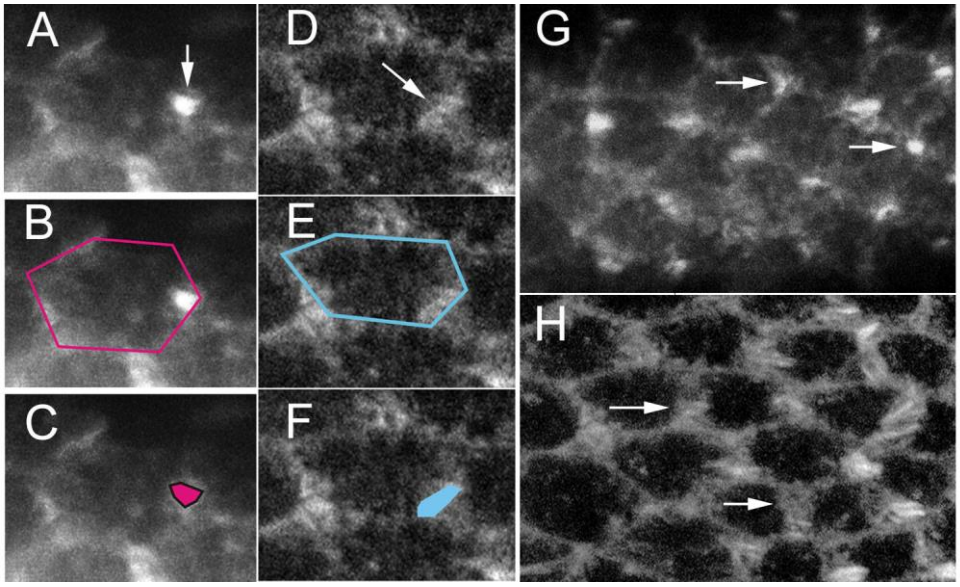

Figure S4. *mwh* mutations result in an increased area where F-actin accumulation is seen. Panels ABC are of an *ap>actin-GFP* cell imaged right around the time of hair initiation. The arrow in A points to the site where F-actin accumulation is seen. In B the outline of the cell is marked in pink and in C the area with increased F-actin staining is marked. Image J was used to measure the areas delimitated in B and C. Panels D, E, F are equivalent for a *ap>actin-GFP*; *mwh* cell. In this case the cell outline and region of increased actin accumulation are marked in blue. In G and H are examples of larger fields that illustrate that only a fraction of the cells in any wing region are useful for such measurements (arrows).

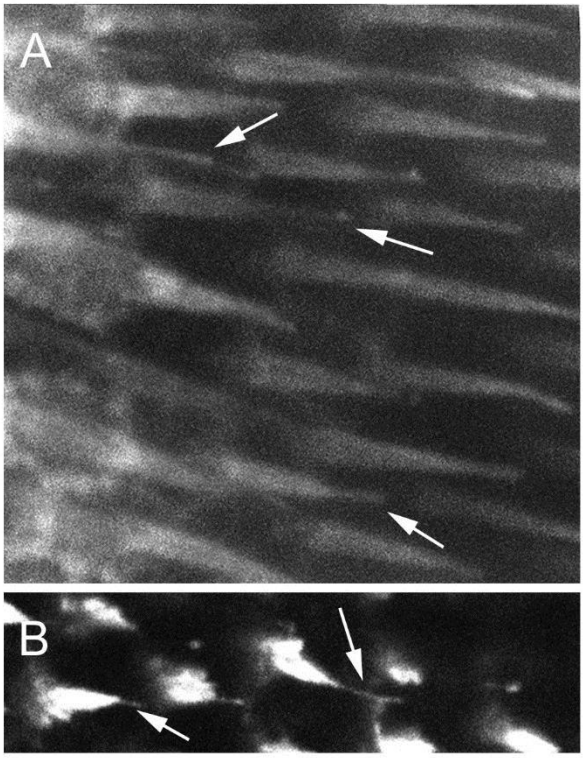

Figure S5. Growing hairs have long thin extensions when observed by in vivo imaging. An image of *ap>MCD8-GFP* pupal wing cells (A). The arrows point to thin extensions at the distal end of hairs. In some cases a “blob” is seen at the tip. An image of *ap>actin-GFP* pupal wing cells B). The arrows point to the thin distal extensions.

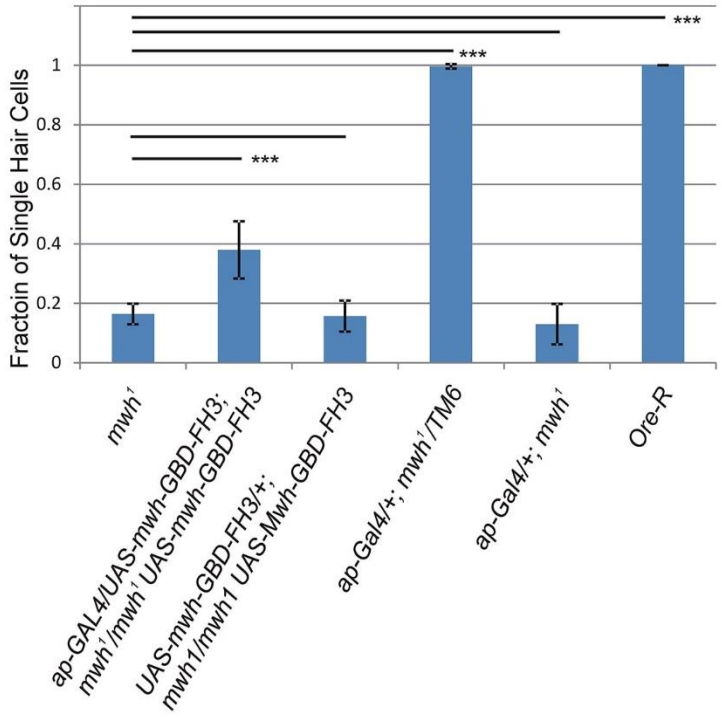

Figure S6. The Mwh-GBD-FH3 fragment shows substantial rescue activity. The fraction of cells that formed a single hair is shown. The region scored was the proximal part of the A cell (most anterior region of the wing) on the dorsal surface. A t-test was used to compare the fraction of single hair cells for various genotypes compared to *mwh*1 homozygotes. *** indicates $p<0.001$. The error bar shows the standard deviation for the sample. Note the partial rescue of the mutant phenotype when *ap-Gal4* drives the expression of *mwh-GBD-FH3*.

Figure S7. Purification of Mwh-GBD-FH3 and Dia-GBD-FH3. A pair of commassie blue stained gels are shown. One shows two lanes of the purified Mwh-GBD-FH3 protein (arrow) and one lane of a molecular weight standard and the other two lanes and the purified Dia-GBD-FH3 protein (arrow) and one lane of molecular weight standards.

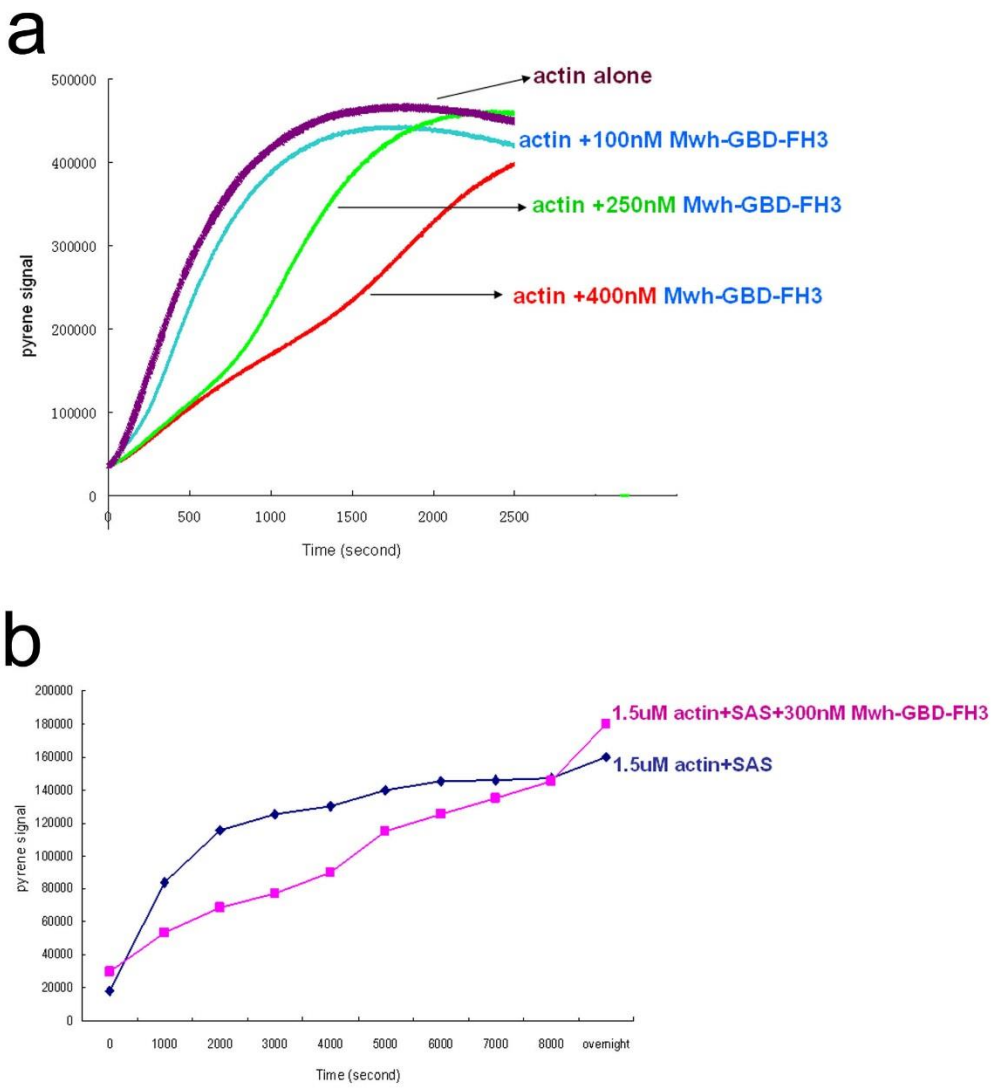

Figure S8. Mwh-GBD-FH3 inhibits the rate but not the extent of F-actin assembly at steady state. In these experiments the reaction was run for a much longer time than in our standard experiments. Although the initial rate of polymerization was slowed by Mwh-GBD-FH3 after a long time the intensity of pyrenyl-actin-flourescence was similar with and without Mwh-GBD-FH3.

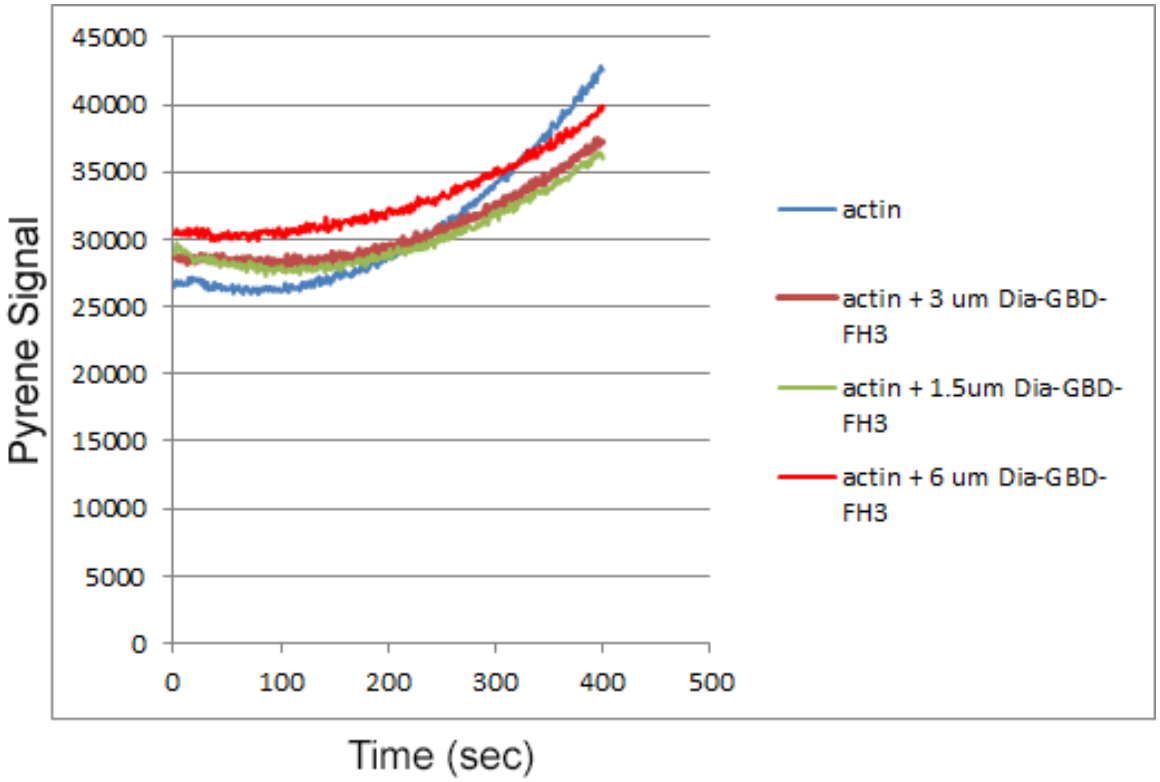

Figure S9. The Dia-GBD-FH3 protein fragment does not inhibit actin assembly.

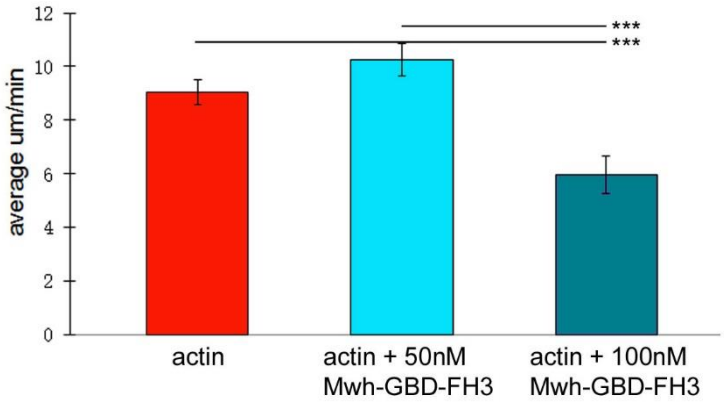

Figure S10. Mwh-GBD-FH3 inhibits the rate of elongation of actin filaments. The rate of actin filament elongation was measured in TIRF experiments and the data plotted. No significant difference was seen between no Mwh-GBD-FH3 and a low dose (50nm) but at 100nM the rate of elongation was significantly reduced. *** indicates a significant difference with a $p < 0.001$.

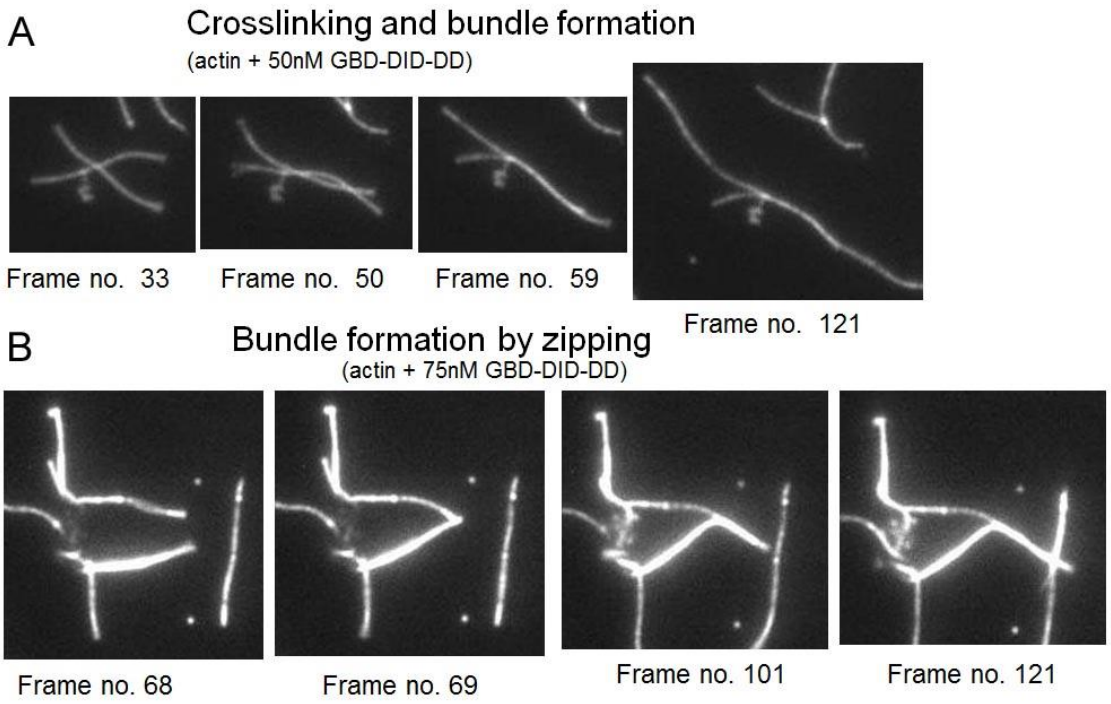

Figure S11. Several different modes of actin filament interaction and bundling are shown. "The cross-linking and alignment of filaments is shown in A. The zippering of filaments is shown in B.

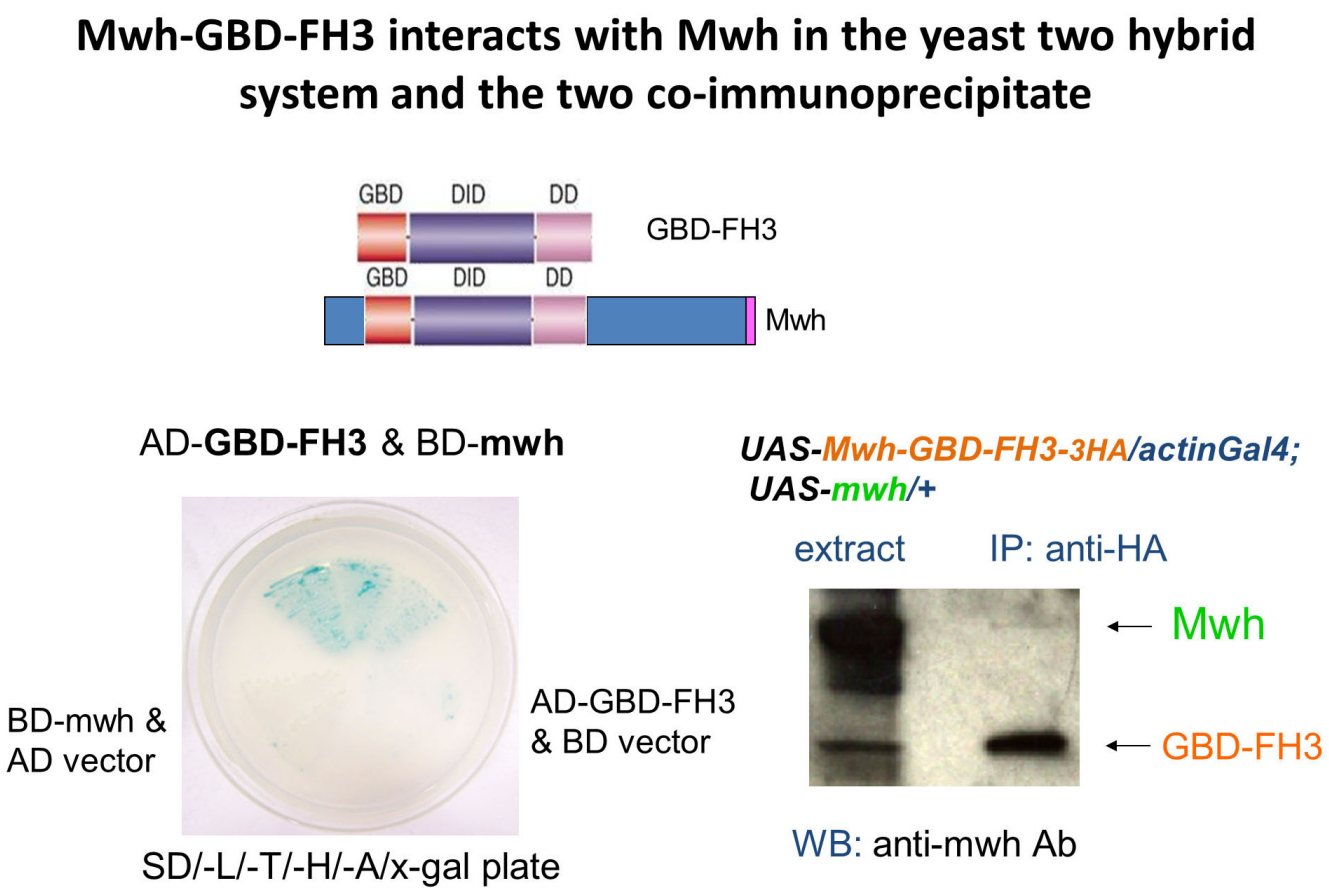

Figure S12. Evidence for the idea that Mwh can dimerize. A positive interaction was seen between Mwh and Mwh-GBD-FH3 in the yeast two hybrid system. A weak co-immunopreciptation was seen between Mwh and Mwh-GBD-FH34-HA.

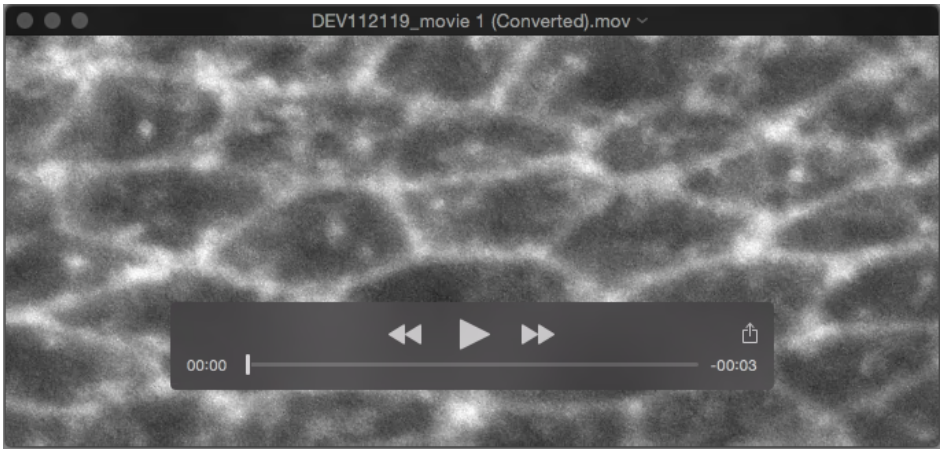

Movie 1. Actin in wild type wing cells prior to hair initation.

Movie 2. Actin and developing hairs in wild type wing cells.

Movie 3. Actin and developing hairs in *mwh* wing cells.

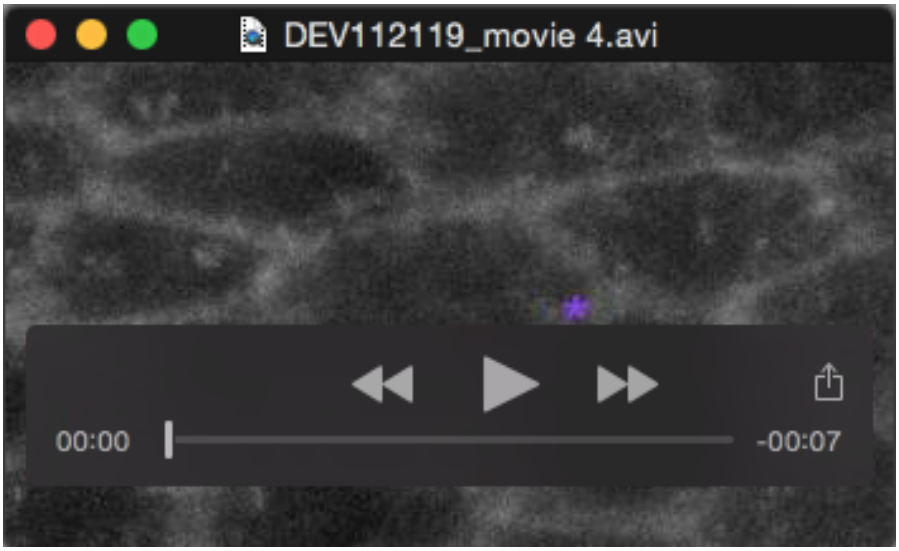

Movie 4. Actin and developing hairs in *mwh* wing cells.

Table S1. The GBD-FH3 domain of Mwh is the most conserved region of the protein.

	amino (1-143) % identity	gbd-fh3 (144-492) % identity	carboxy (493-800) % identity	entire % identity
Drosophila melanogaster	100	100	100	100
Drosophila yakuba	97	99	96	98
Drosophila virilis	67	86	69	74
Bactrocera dorsalis	49	75	51	60
Musca domestica	46	72	51	59
Anopheles gambiae	38	66	32	46
Tribolium castaneum	28	45	21	32
Danaus plexippus	32	43	20	31
Acyrthosiphon pisum	24	37	19	27
Nasonia vitripennis	24	37	18	25
Apis mellifera	25	37	17	23
Pediculus humanus corporis	23	42	13	21
Daphnia pulex	15	30	6	19